Supplemental Information
For

Increased binding of thiophene-based ligands to mercury(II) with water solubilizing functional groups

Austin K. Shigemoto, Abigail A. Killjoy, Julia Dayton,

Carolyn N. Virca, Theresa M. McCormick*

Department of Chemistry, Portland State University, Portland, Oregon 97201, USA.

Table of Contents

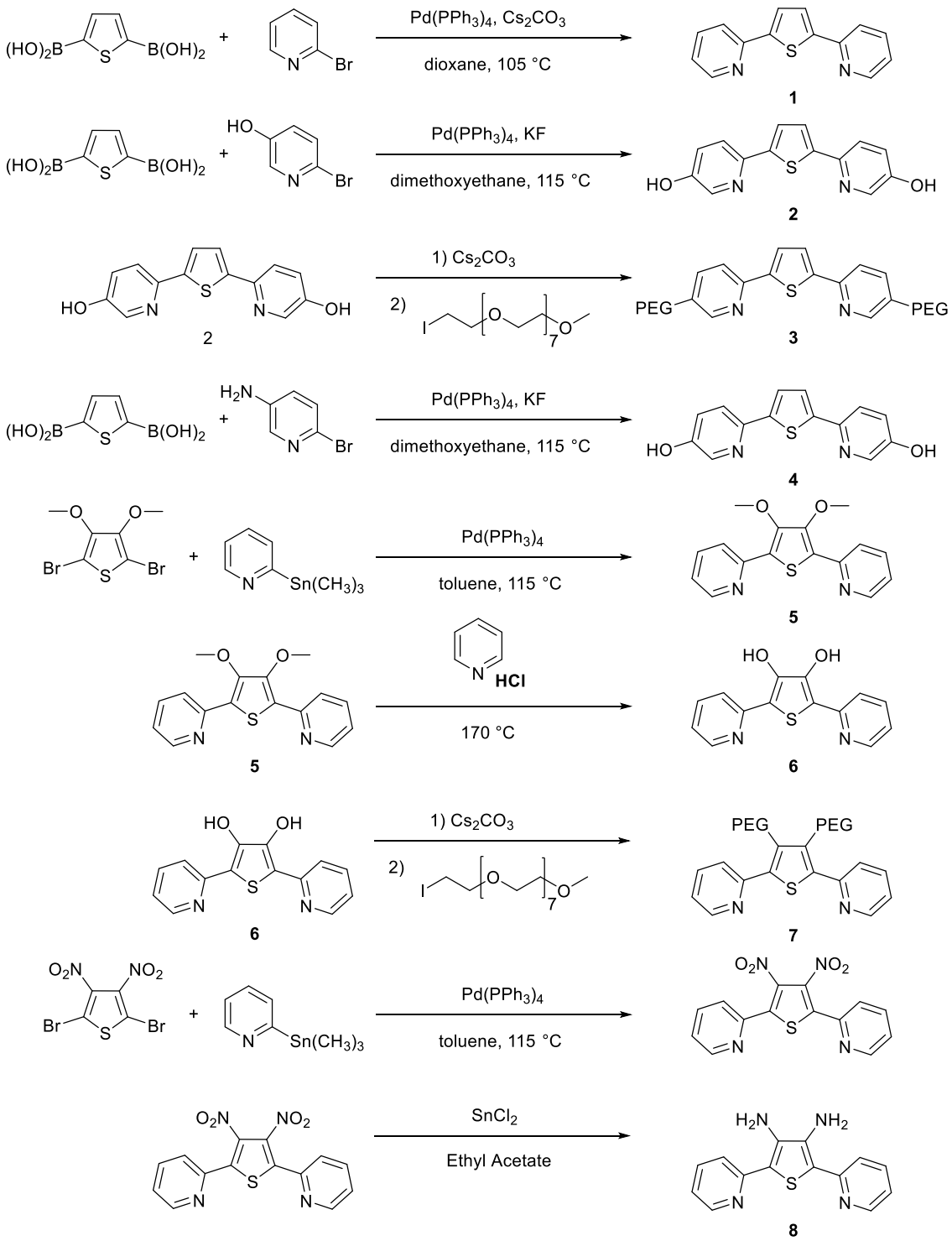

Scheme S1: Synthetic scheme for the synthesis of **1**-**8.**

Table S1: Association constant data obtained from fits of absorption titration data. Stepwise data constants are reported along with the overall binding constant for compounds **1**-**3.**

	K_{11} (M^{-1})	K_{21} (M^{-1})	K_a (M^{-2})
1	6.93×10^1 (± 4 %)	7.70×10^7 (± 9 %)	5.37×10^9 (± 4 %)
2	1.15×10^2 (± 7 %)	3.93×10^8 (± 17 %)	4.52×10^{10} (± 18 %)
3	1.89×10^5 (± 8 %)	7.57×10^5 (± 8 %)	1.43×10^{11} (± 12 %)

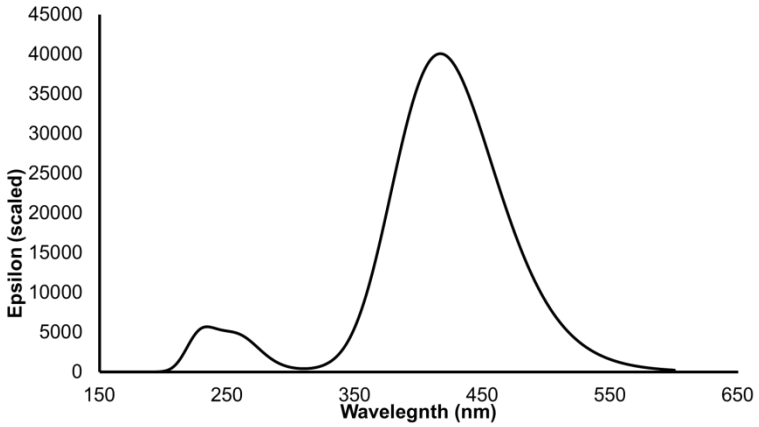

Figure S1: Calculated absorbance spectrum of **2** (0.3 eV FVHM) as determined by TD-DFT calculations using B3Lyp/6-311+G(d) basis set.

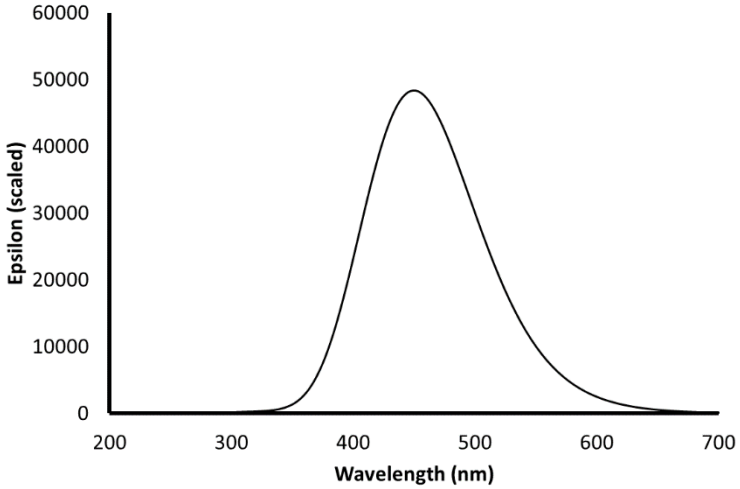

Figure S2: Calculated absorbance spectrum of **3** (0.3 eV FVHM) as determined by TD-DFT calculations using B3Lyp/6-311+G(d) basis set.

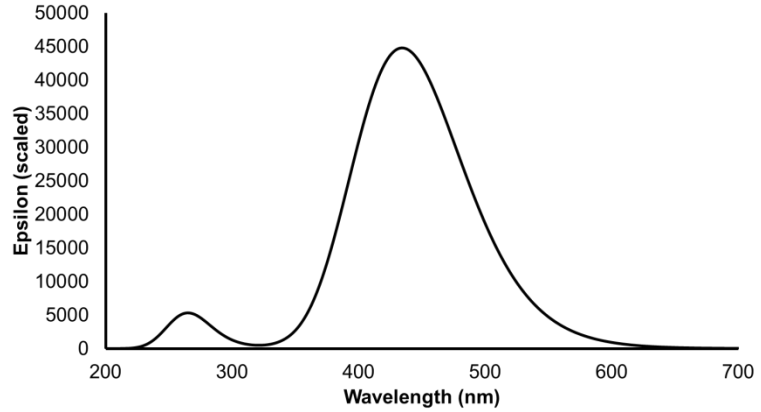

Figure S3: Calculated absorbance spectrum of **4** (0.3 eV FVHM) as determined by TD-DFT calculations using B3Lyp/6-311+G(d) basis set.

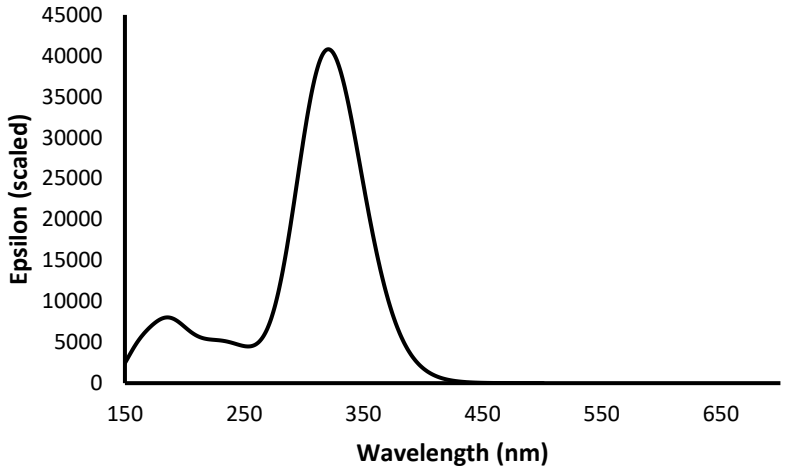

Figure S4: Calculated absorbance spectrum of **5** (0.3 eV FVHM) as determined by TD-DFT calculations using B3Lyp/6-311+G(d) basis set.

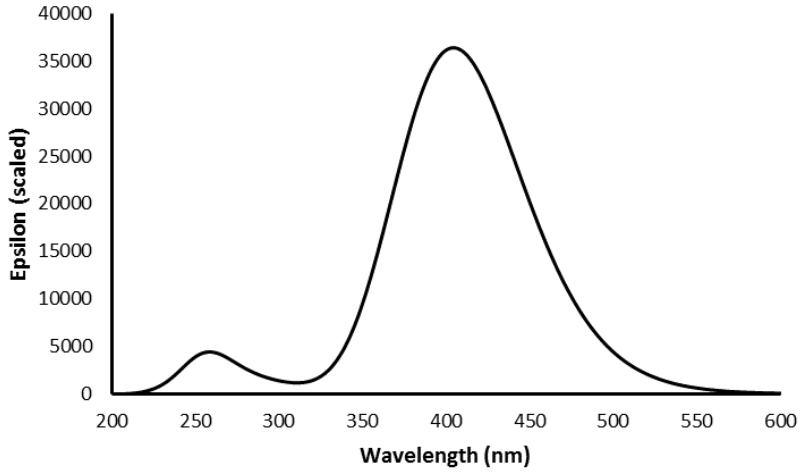

Figure S5: Calculated absorbance spectrum of **6** (0.3 eV FVHM) as determined by TD-DFT calculations using B3Lyp/6-311+G(d) basis set.

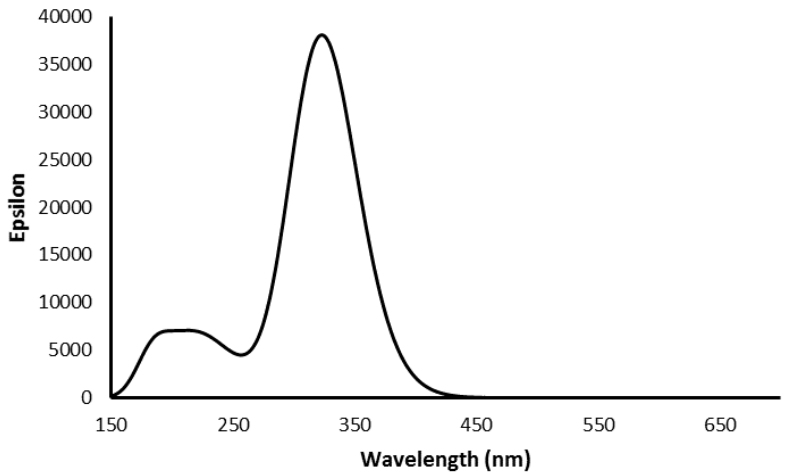

Figure S6: Calculated absorbance spectrum of **7** (0.3 eV FVHM) as determined by TD-DFT calculations using B3Lyp/6-311+G(d) basis set.

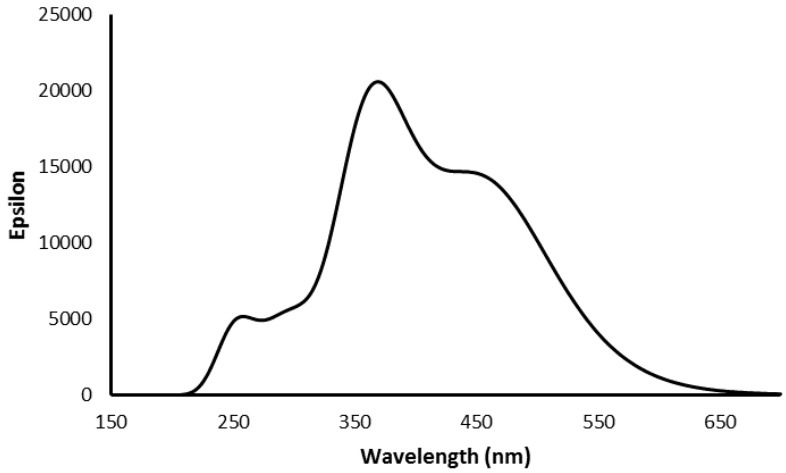

Figure S7: Calculated absorbance spectrum of **8** (0.3 eV FVHM) as determined by TD-DFT calculations using B3Lyp/6-311+G(d) basis set.

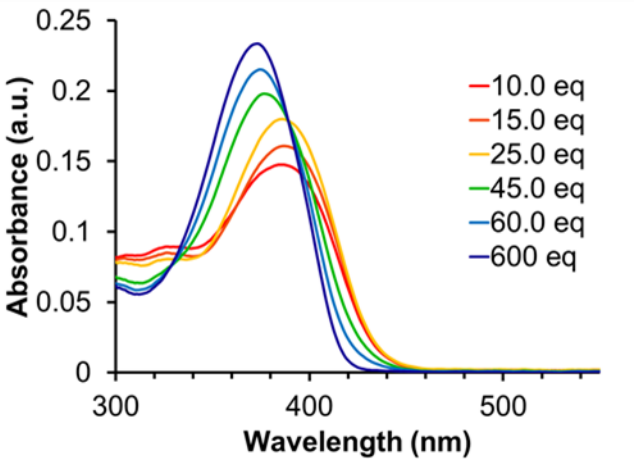

Figure S8: Change in absorption spectrum of **2** (1×10^{-5} M) in response to mercury(II) forming the second product in CH_3CN.

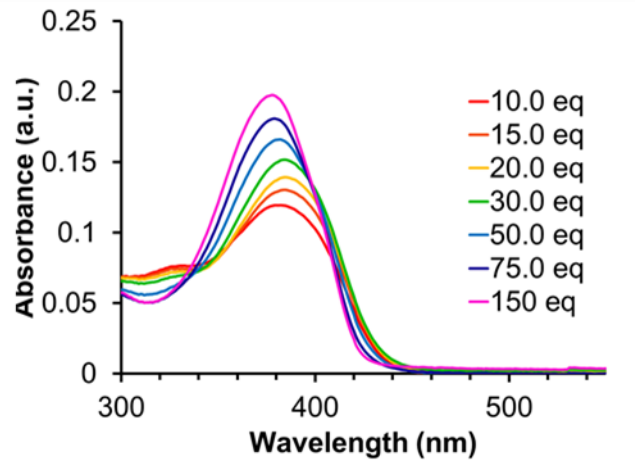

Figure S9: Change in absorption spectrum of **3** in response to mercury(II) forming the second product in CH_3CN.

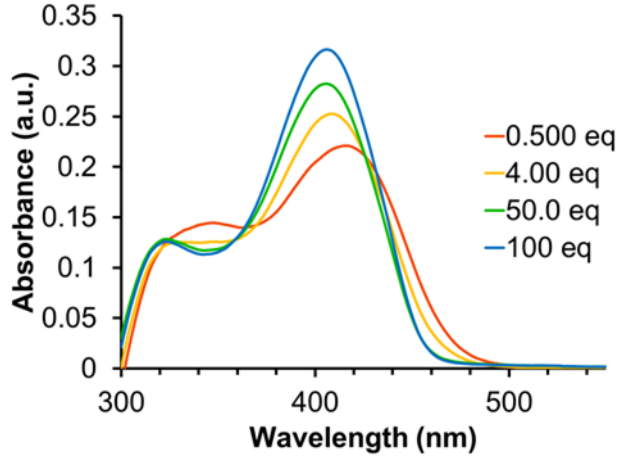

Figure S10: Change in absorption spectrum of **4** in response to mercury(II) forming the second product in CH_3CN.

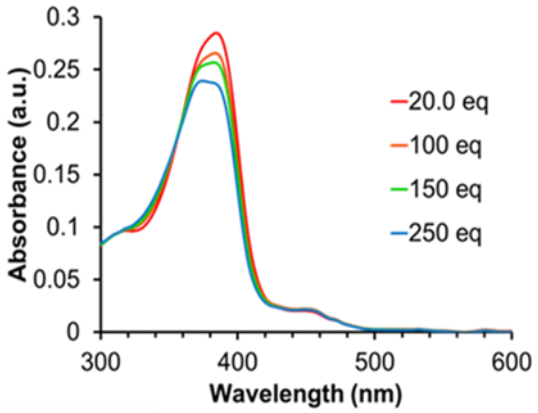

Figure S11: Change in absorption spectrum of **5** in response to mercury(II) forming the second product in CH_3CN.

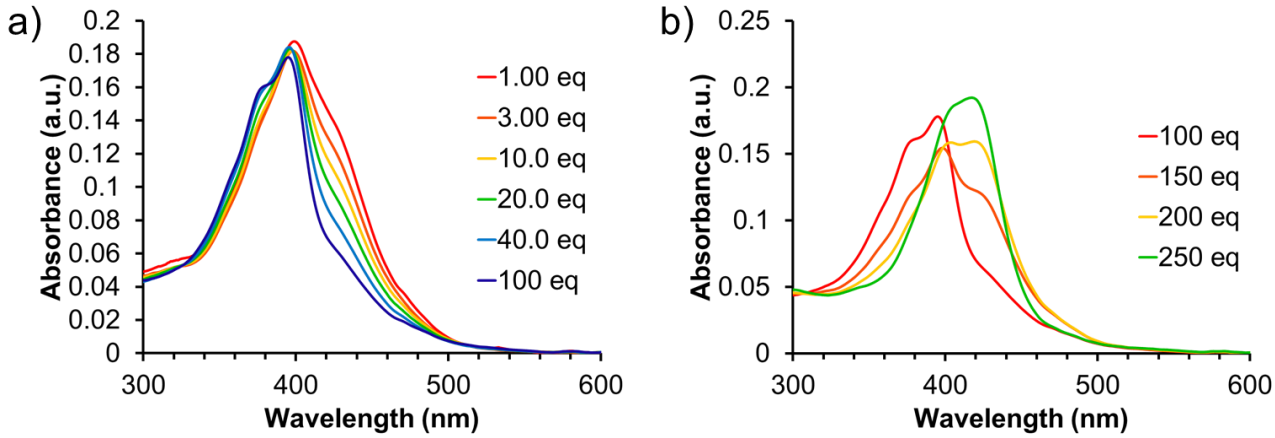

Figure S12: Change in absorption spectrum of **6** in response to mercury(II) forming the second (a), and third (b) product in CH_3CN.

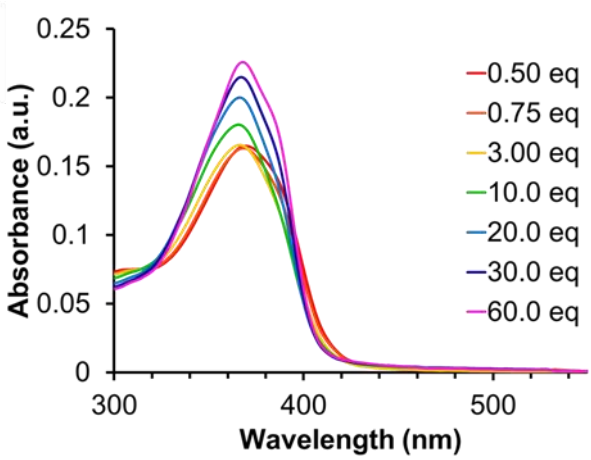

Figure S13: Change in absorption spectrum of **7** in response to mercury(II) forming the second product in CH_3CN.

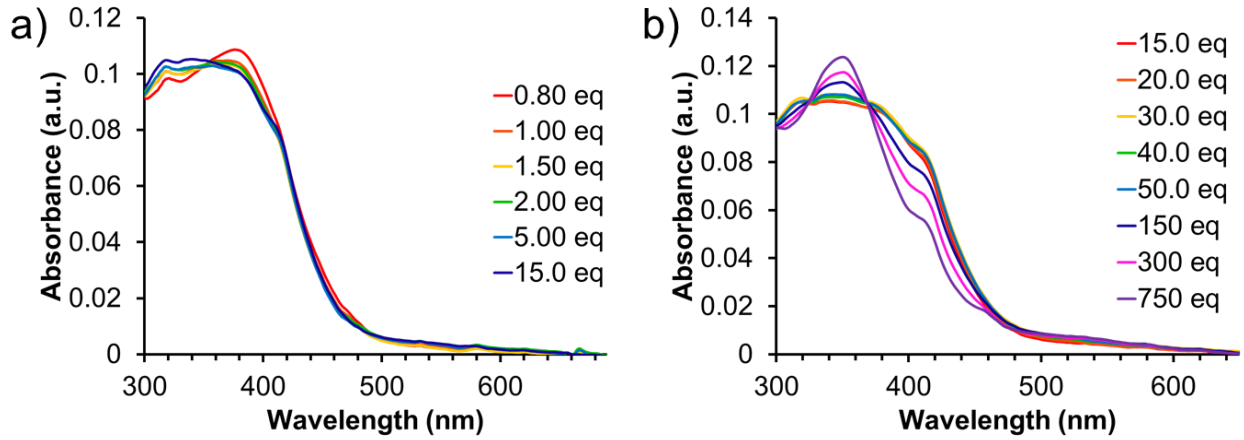

Figure S14: Change in absorption spectrum of **8** in response to mercury(II) forming the second (a), and third (b) product in CH_3CN.

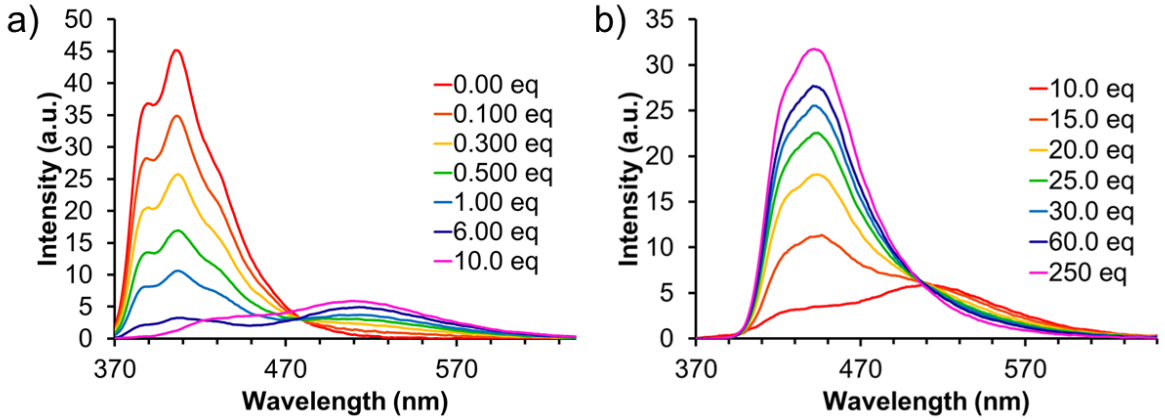

Figure S15: Change in emission spectrum of **2** in response to mercury(II) to form the first (a) and second (b) product in CH_3CN.

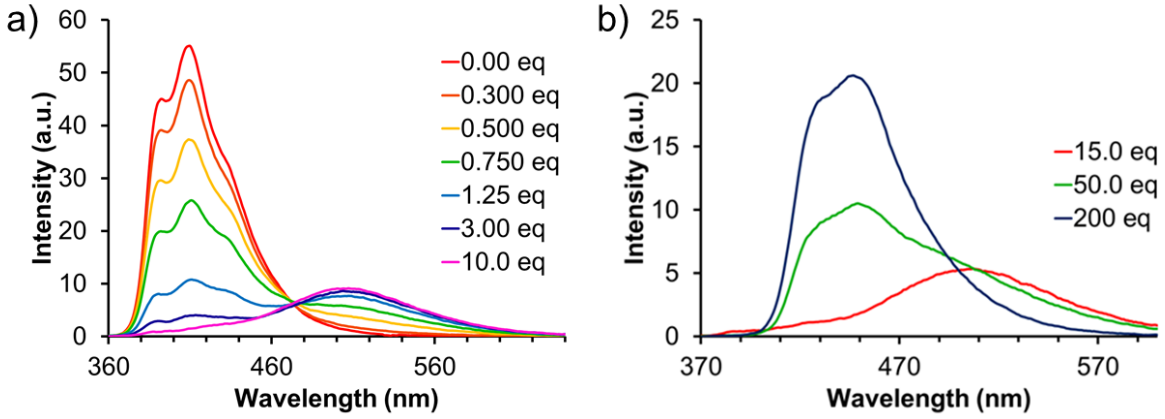

Figure S16: Change in emission spectrum of **3** in response to mercury(II) to form the first (a) and second (b) product in CH_3CN.

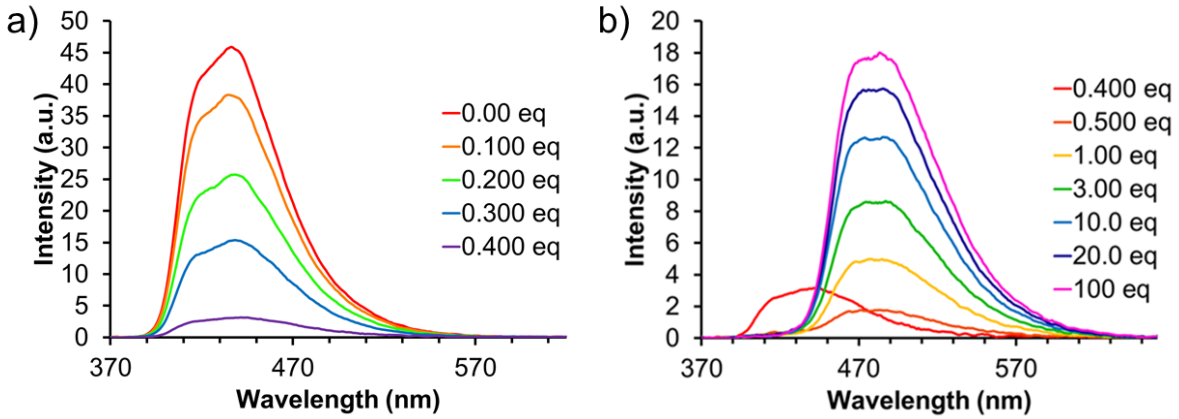

Figure S17: Change in emission spectrum of **4** in response to mercury(II) to form the first (a) and second (b) product in CH_3CN.

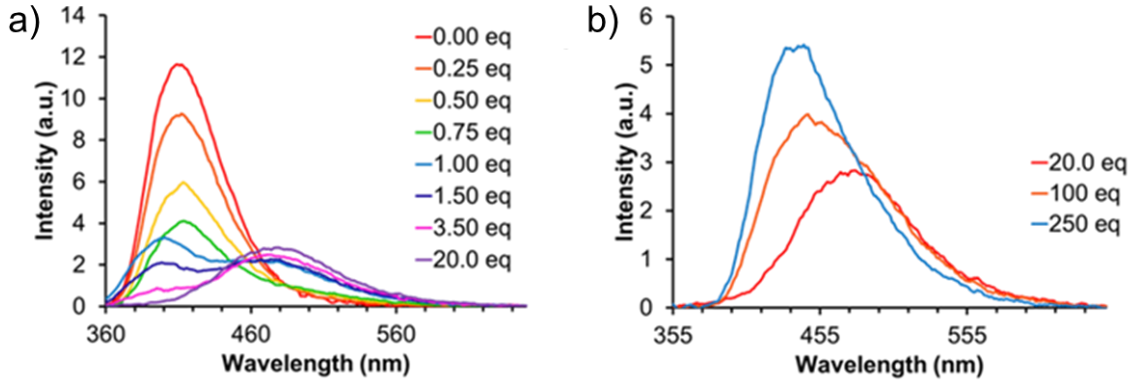

Figure S18: Change in emission spectrum of **5** in response to mercury(II) to form the first (a) and second (b) product in CH_3CN.

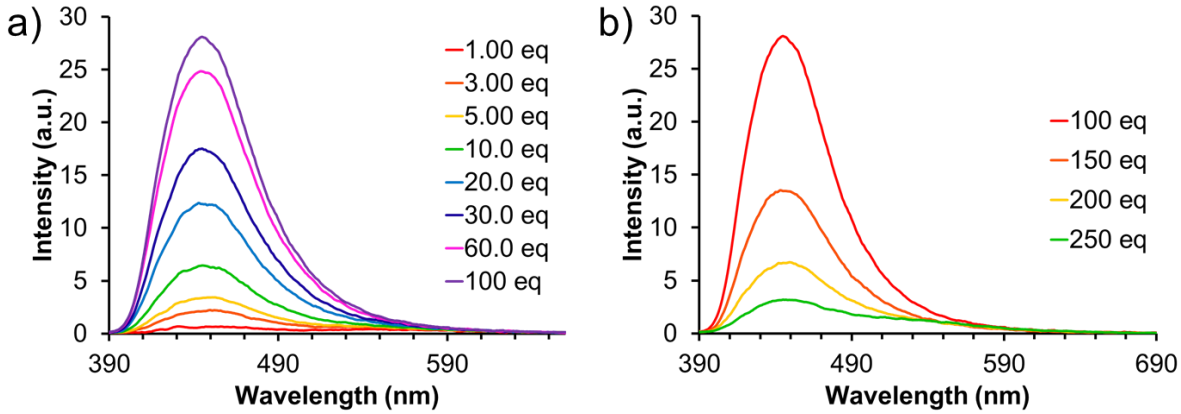

Figure S19: Change in emission spectrum of **6** in response to mercury(II) to form the second (a) and third (b) product in CH_3CN.

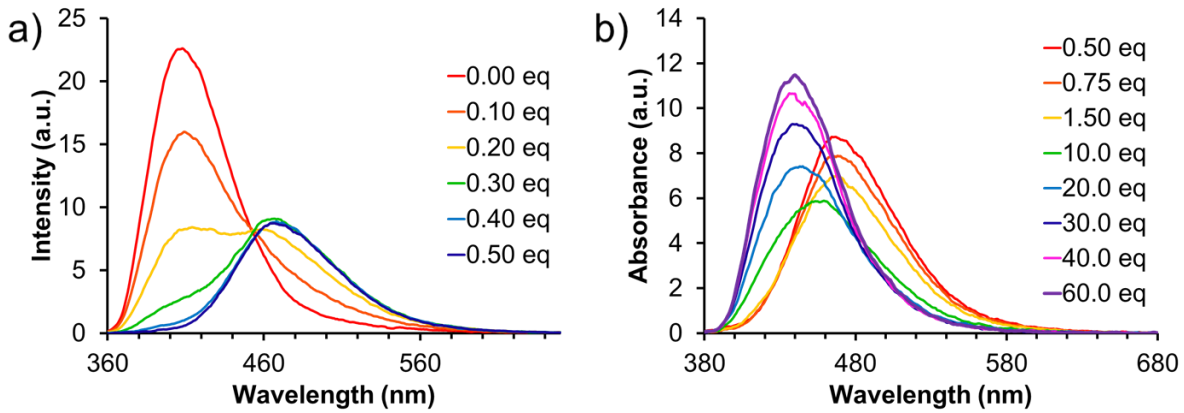

Figure S20: Change in emission spectrum of **7** in response to mercury(II) to form the first (a) and second (b) product in CH_3CN.

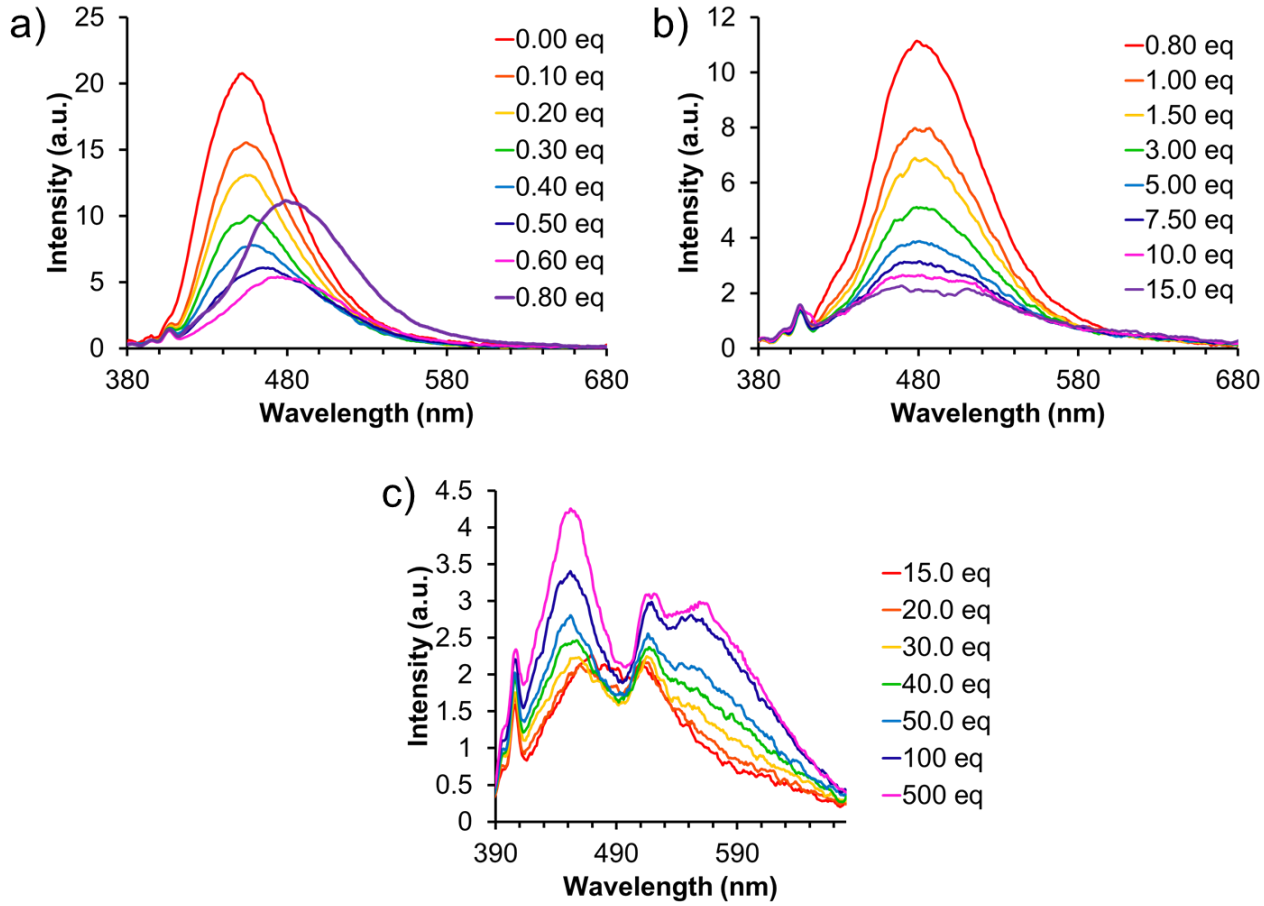

Figure S21: Change in emission spectrum of **8** in response to mercury(II) to form the first (a), second (b), and third (c) product in CH_3CN.

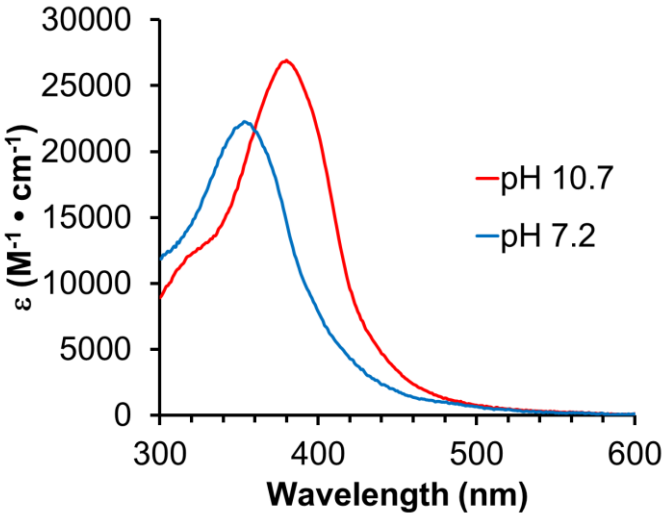

Figure S22: Absorption spectrum of **2** (1×10^{-5} M) under neutral and basic conditions.

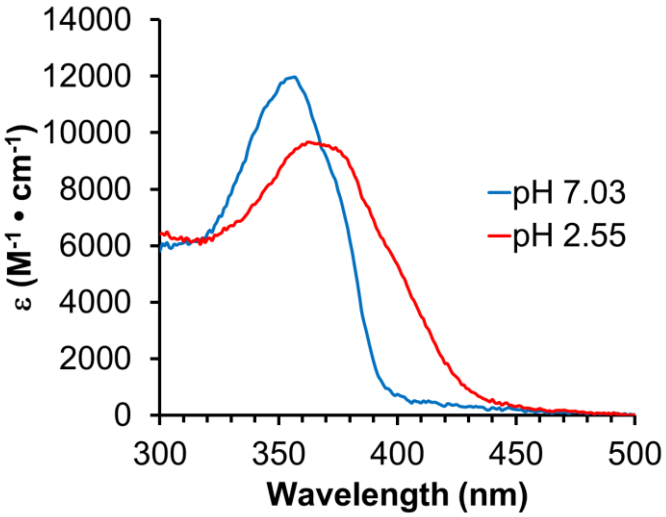

Figure S23: Absorption spectrum of **3** (1×10^{-5} M) under neutral and acidic conditions.

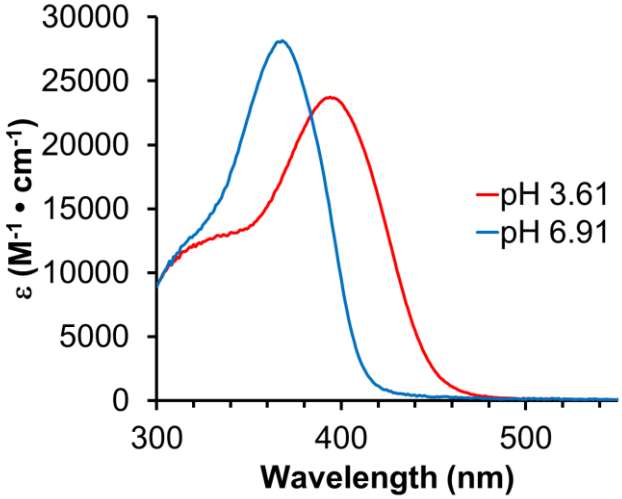

Figure S24: Absorption spectrum of **4** (1×10^{-5} M) in acidic and neutral conditions.

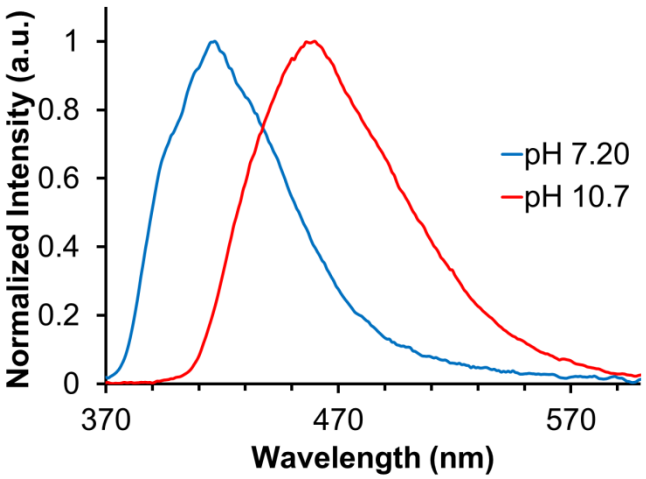

Figure S25: Emission spectrum of **2** (1×10^{-5} M) in basic and neutral conditions.

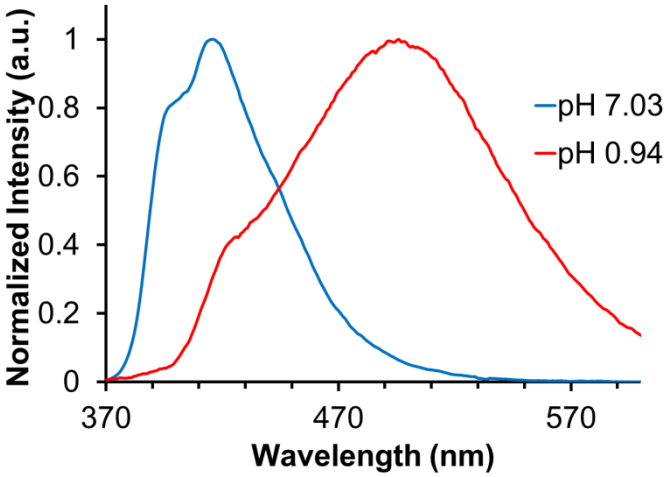

Figure S26: Emission spectrum of **3** (1×10^{-5} M) under acidic and neutral conditions.

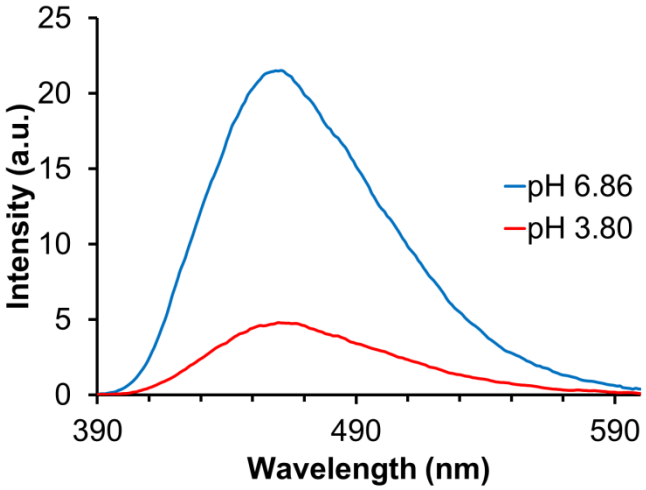

Figure S27: Emission spectrum of **4** (1×10^{-5} M) under acidic and neutral conditions.

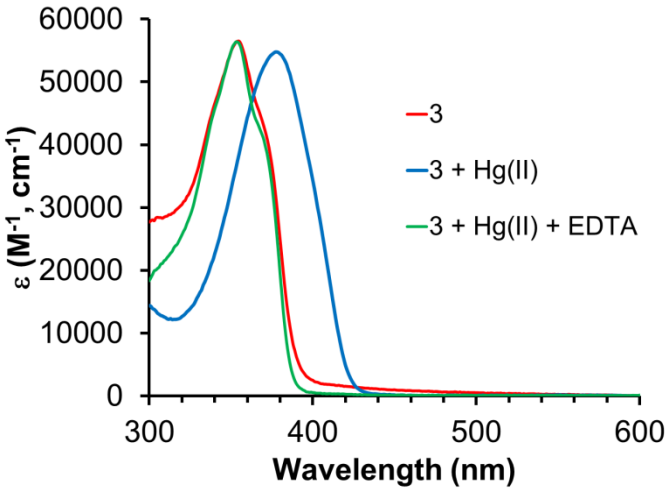

Figure S28: Absorption spectrum a solution of **3** prior to the addition of mercury(II) (red), after the addition of mercury(II) (blue), and subsequent addition of EDTA (green).

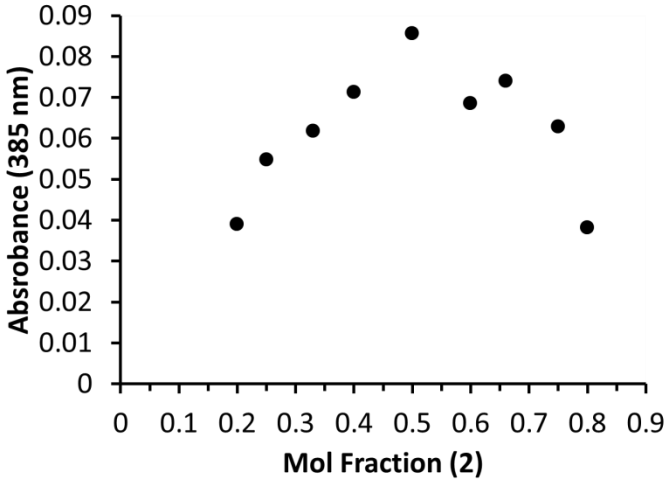

Figure S29: Job's plot for compound **2** with mercury(II) perchlorate, obtained from absorbance spectra.

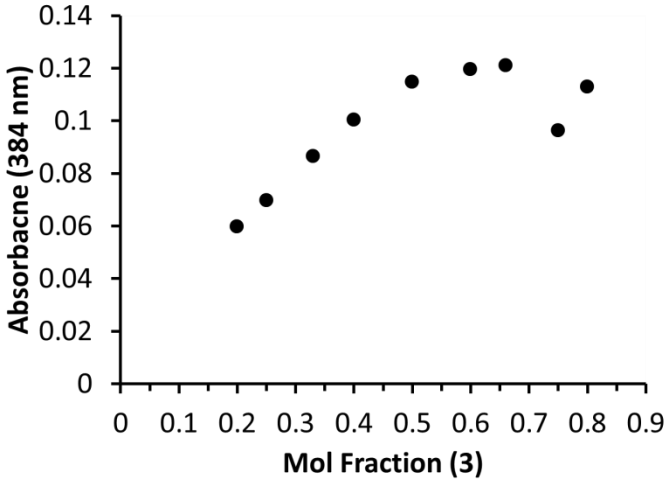

Figure S30: Job's plot for compound **3** with mercury(II) perchlorate, obtained from absorbance spectra.

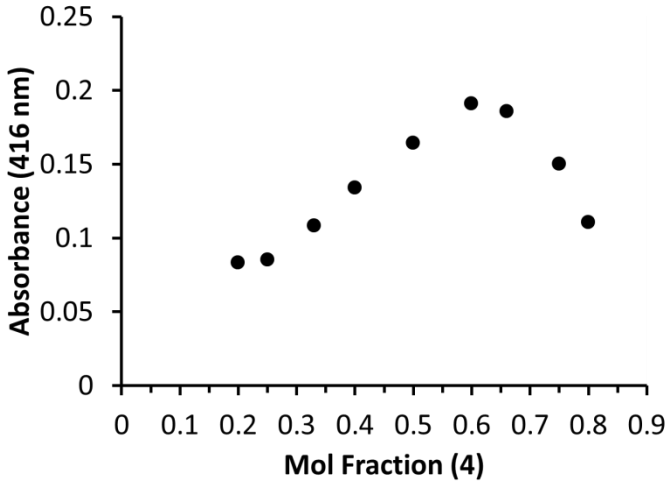

Figure S31: Job's plot for compound **4** with mercury(II) perchlorate, obtained from absorbance spectra.

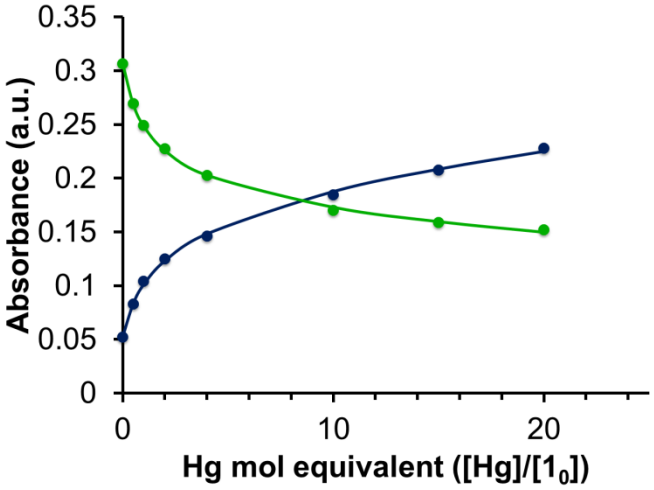

Figure S32: Absorption titration data (dots) overlaid with calculated fit (line) for compound **1**. Titration data was fit for the change in absorbance at both 368 nm (blue) and 342 nm (green) to obtain binding constants. Fit was obtained using the Thordarson Program for the 2:1 Nelder-Mead model.

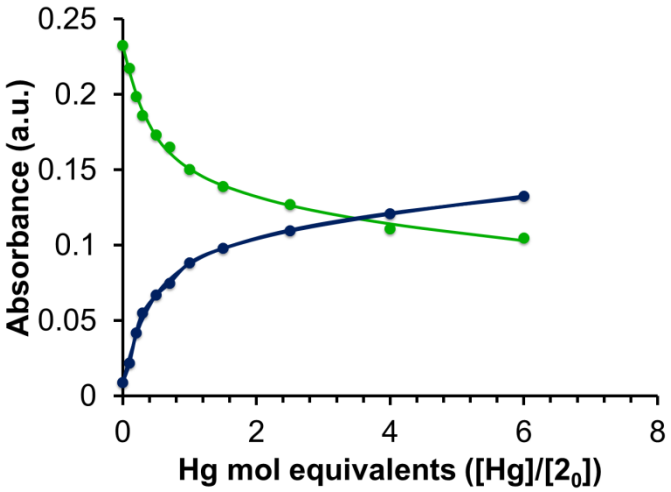

Figure S33: Absorption titration data (dots) overlaid with calculated fit (line) for compound **2**. Titration data was fit for the change in absorbance at both 385 nm (blue) and 351 nm (green) to obtain binding constants. Fit was obtained using the Thordarson Program for the 2:1 Nelder-Mead model.

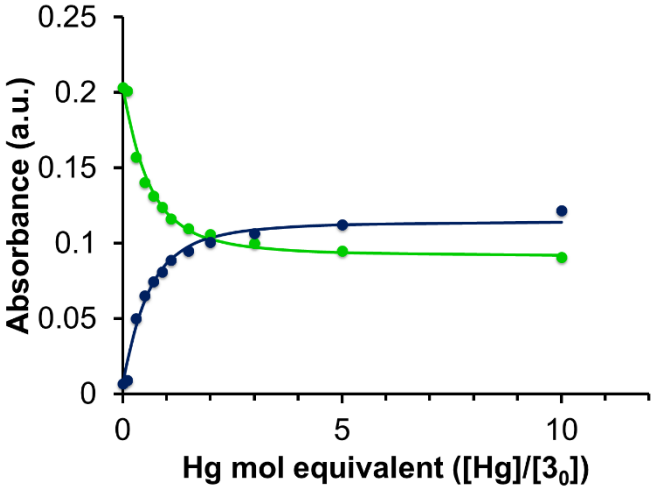

Figure S34: Absorption titration data (dots) overlaid with calculated fit (line) for compound **3**. Titration data was fit for the change in absorbance at both 392 nm (blue) and 349 nm (green) to obtain binding constants. Fit was obtained using the Thordarson Program for the 2:1 Nelder-Mead model, for non-cooperative binding.

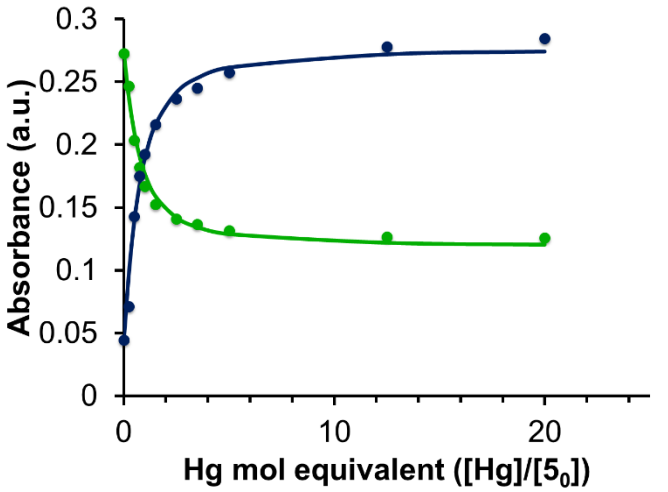

Figure S35: Absorption titration data (dots) overlaid with calculated fit (line) for compound **5**. Titration data was fit for the change in absorbance at both 385 nm (blue) and 343 nm (green) to obtain binding constants. Fit was obtained using the Thordarson Program for the 2:1 Nelder-Mead model, for non-cooperative binding.

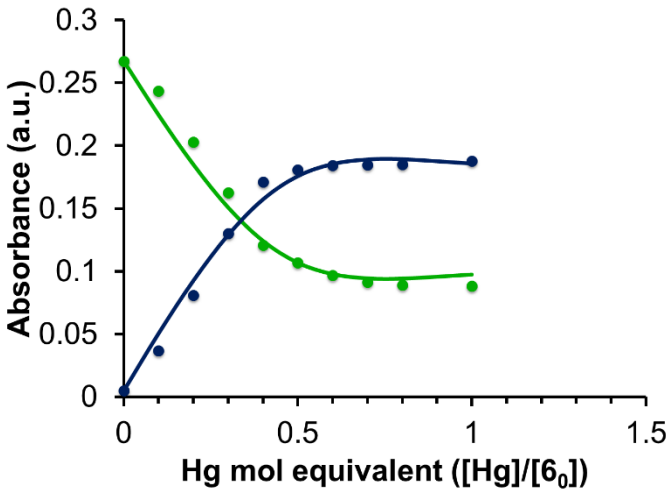

Figure S36: Absorption titration data (dots) overlaid with calculated fit (line) for compound **6**. Titration data was fit for the change in absorbance at both 399 nm (blue) and 354 nm (green) to obtain binding constants. Fit was obtained using the Thordarson Program for the 2:1 Nelder-Mead model, for non-cooperative binding.

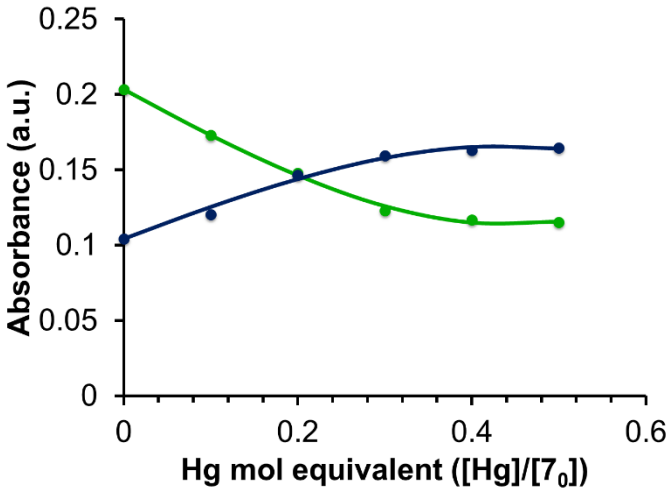

Figure S37: Absorption titration data (dots) overlaid with calculated fit (line) for compound **7**. Titration data was fit for the change in absorbance at both 369 nm (blue) and 345 nm (green) to obtain binding constants. Fit was obtained using the Thordarson Program for the 2:1 Nelder-Mead model, for non-cooperative binding.

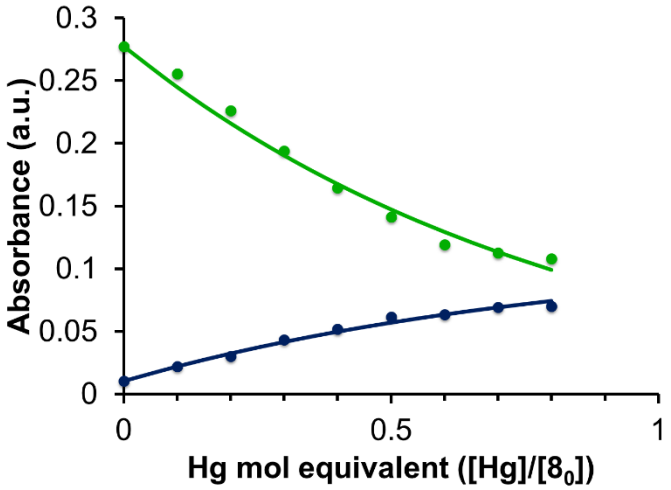

Figure S38: Absorption titration data (dots) overlaid with calculated fit (line) for compound **8**. Titration data was fit for the change in absorbance at both 392 nm (blue) and 349 nm (green) to obtain binding constants. Fit was obtained using the Thordarson Program for the 2:1 Nelder-Mead model, for non-cooperative binding.

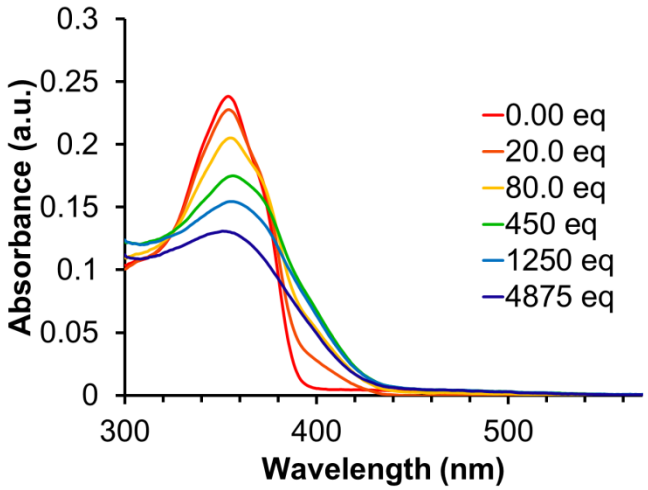

Figure S39: Absorption titration of **2** with mercury(II) in 50:50 $CH_3CN:H_2O$.

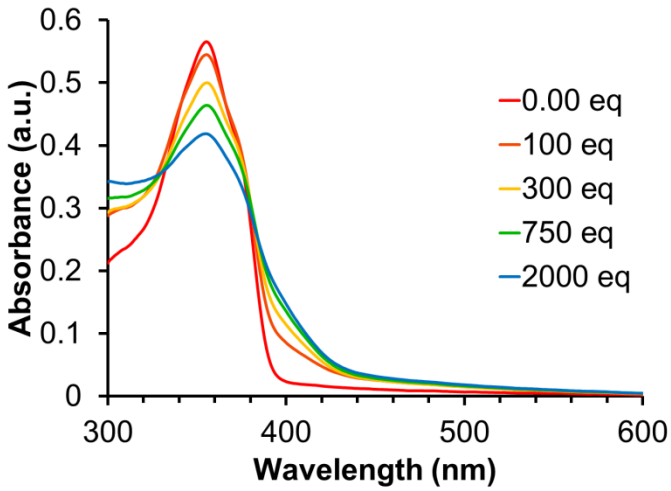

Figure S40: Absorption titration of **3** with mercury(II) in 50:50 $CH_3CN:H_2O$

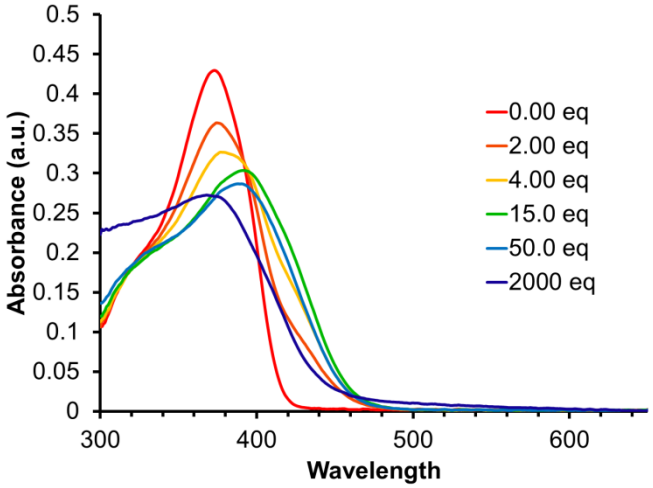

Figure S41: Absorption titration of **4** with mercury(II) in 50:50 $CH_3CN:H_2O$

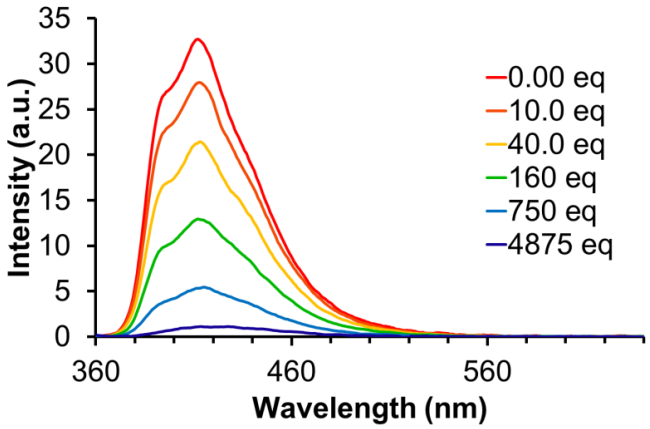

Figure S42: Emission titration of **2** with mercury(II) in 50:50 $CH_3CN:H_2O$.

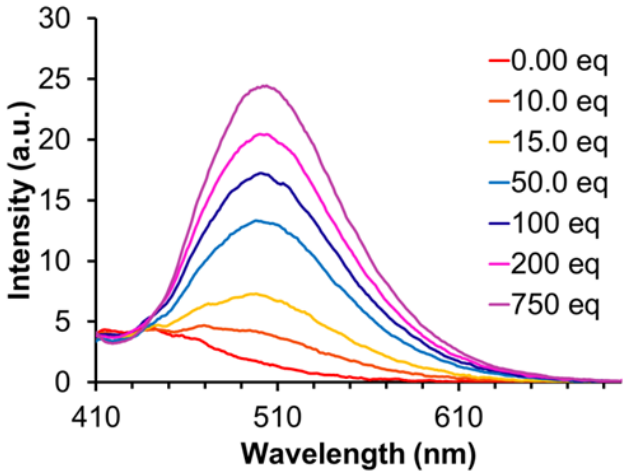

Figure S43: Emission titration of **3** with mercury(II) in 50:50 $CH_3CN:H_2O$.

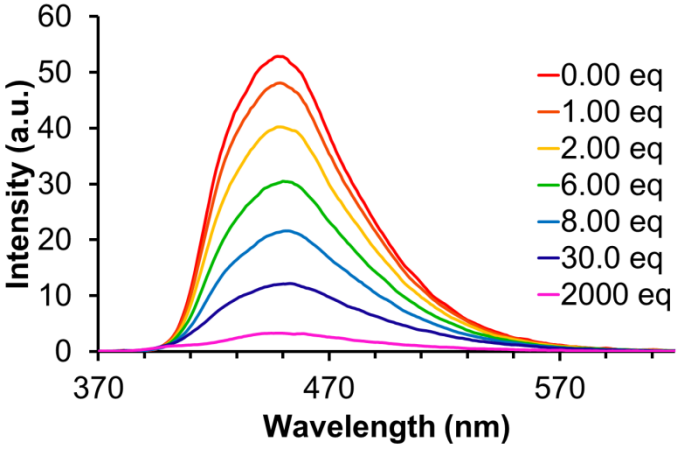

Figure S44: Emission titration of **4** with mercury(II) in 50:50 $CH_3CN:H_2O$.

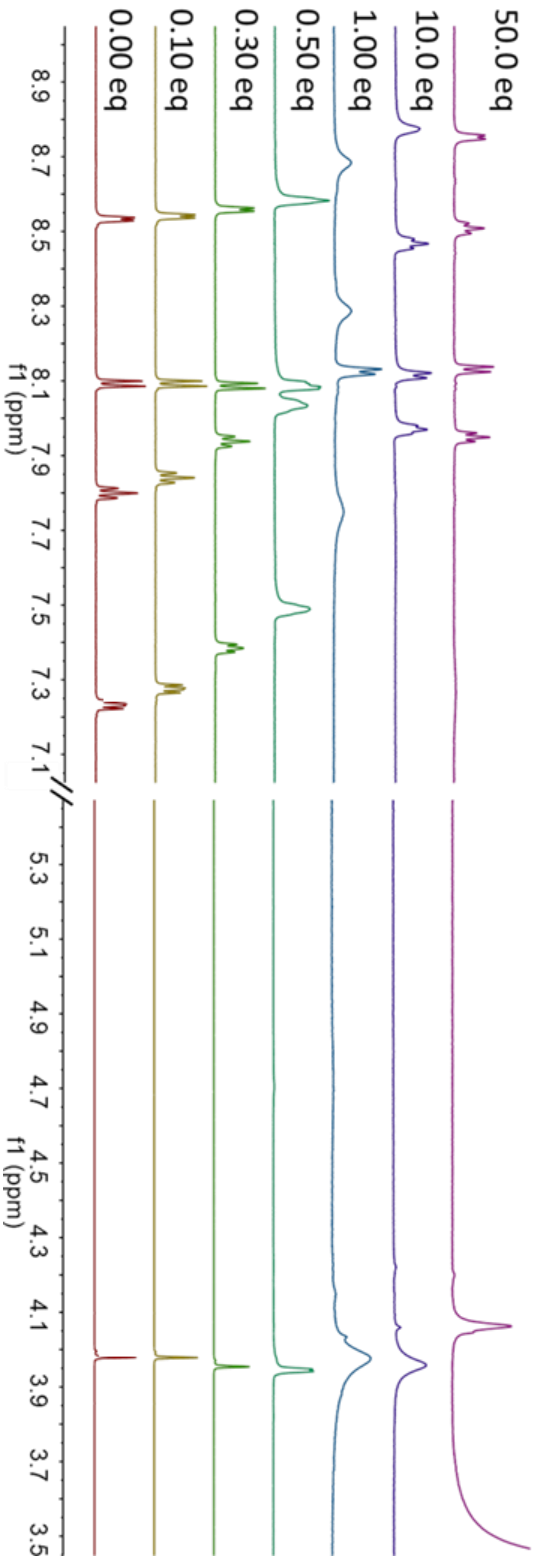

Figure S45: ^{1}H NMR titration of **5** at 4×10^{-3} M with increasing amounts of mercury(II) in CD_3CN.

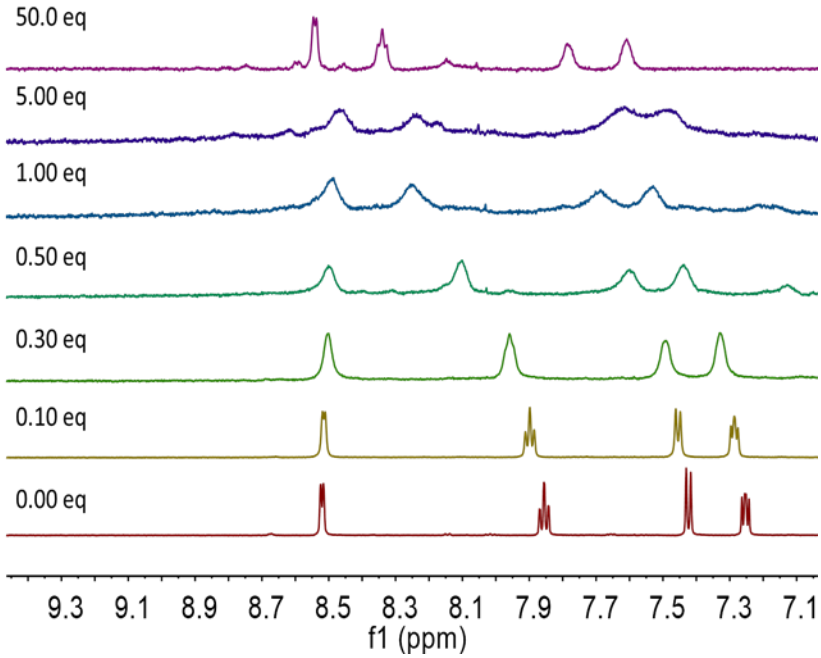

Figure S46: ^{1}H NMR titration of **6** at 4×10^{-3} M with increasing amounts of mercury(II) in CD_3CN.

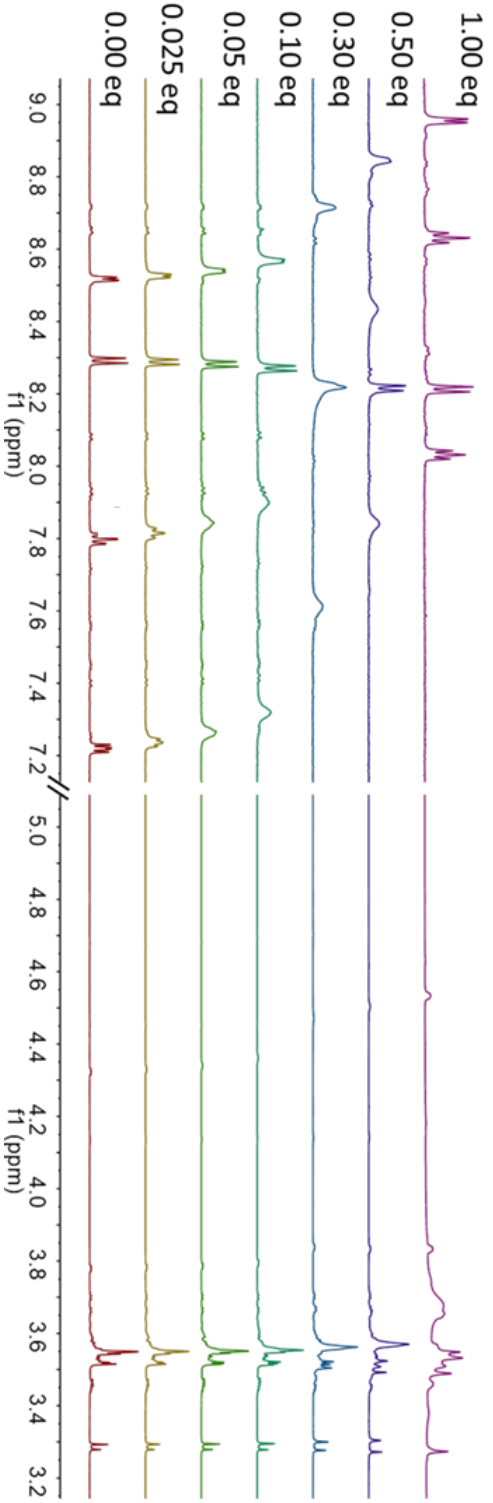

Figure S47: ^{1}H NMR titration of **7** at 4×10^{-3} M with increasing amounts of mercury(II) in CD_3CN.

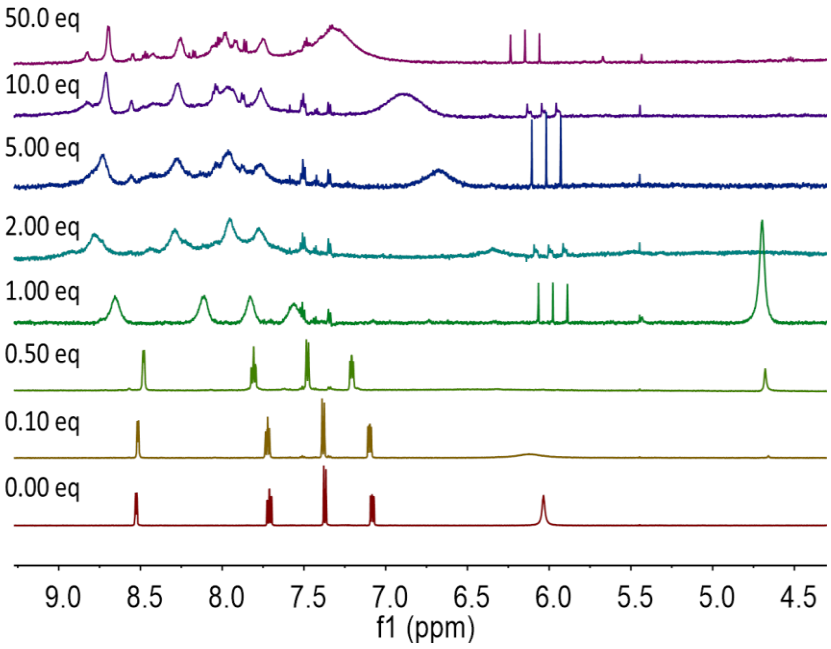

Figure S48: ^{1}H NMR titration of **8** at 4 × 10^{-3} M with increasing amounts of mercury(II) in CD_3CN.

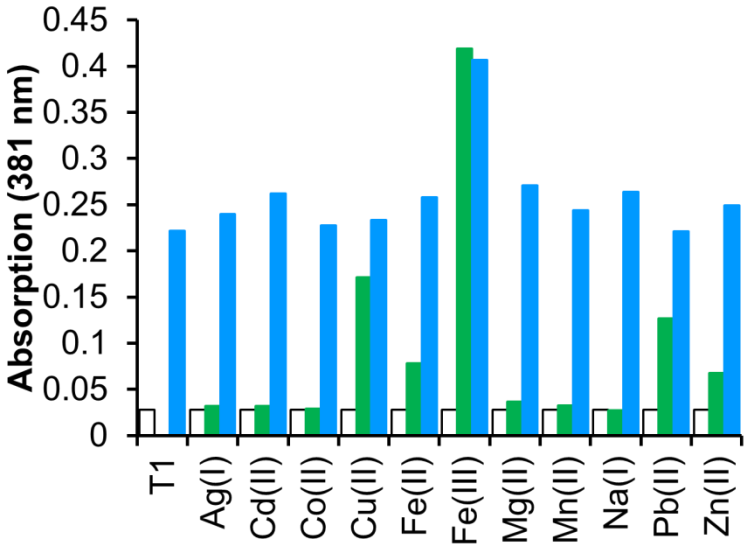

Figure S49: Absorption at 381 nm of **5** (white bars), after the addition of 5 eq. of metal ion (green bars), and subsequent addition of 5 eq. of mercury(II) perchlorate (blue bars) in CH_3CN.

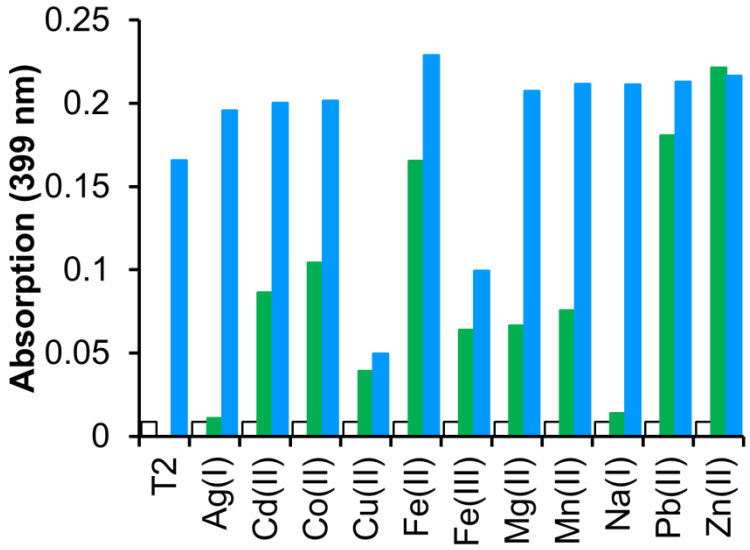

Figure S50: Absorption at 399 nm of **6** (white bars), after the addition of 5 eq. of metal ion (green bars), and subsequent addition of 5 eq. of mercury(II) perchlorate (blue bars) in CH_3CN.

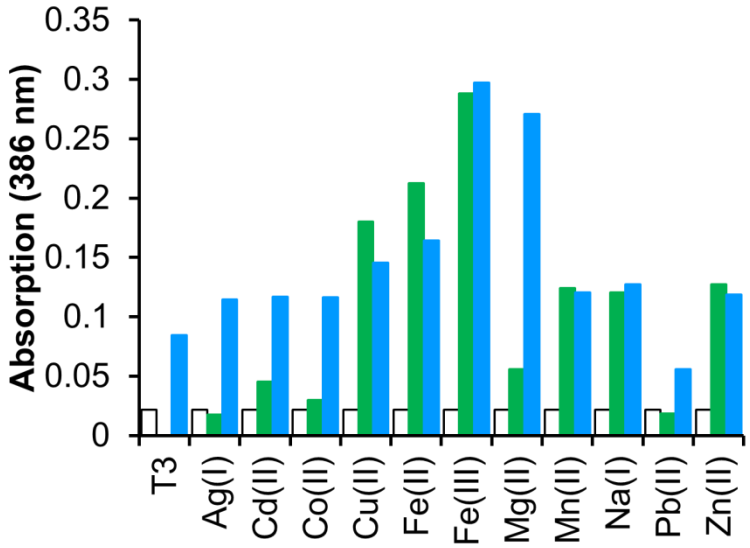

Figure S51: Absorption at 386 nm of **7** (white bars), after the addition of 5 eq. of metal ion (green bars), and subsequent addition of 5 eq. of mercury(II) perchlorate (blue bars) in CH_3CN.

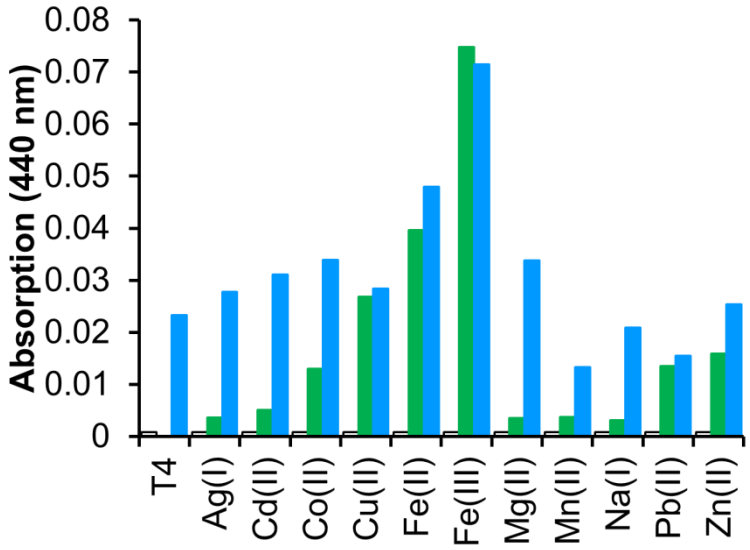

Figure S52: Absorption at 381 nm of **8** (white bars), after the addition of 5 eq. of metal ion (green bars), and subsequent addition of 5 eq. of mercury(II) perchlorate (blue bars) in CH_3CN.